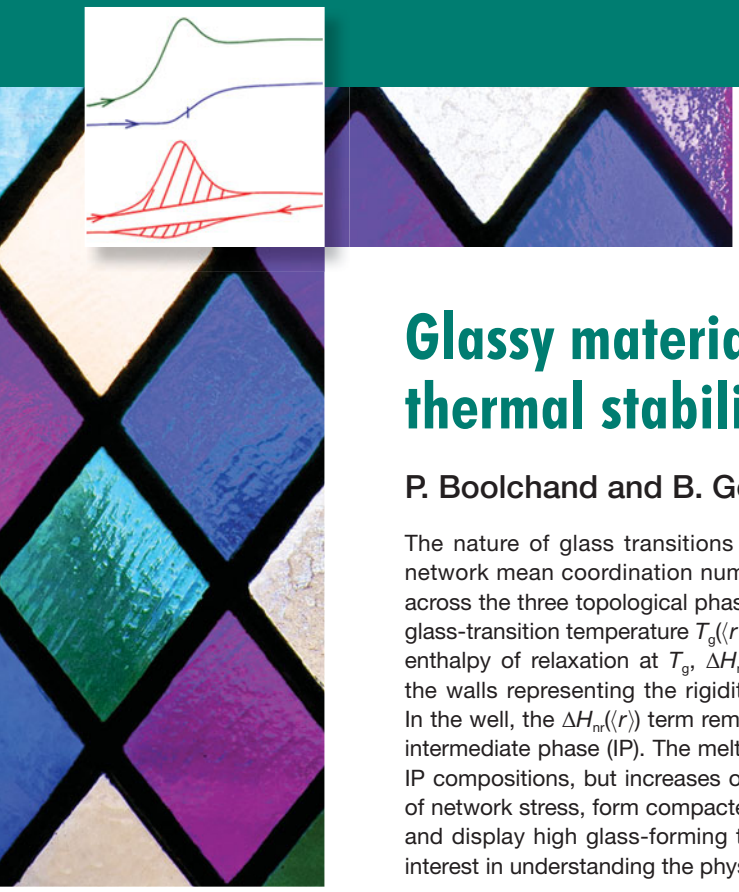

Glassy materials with enhanced thermal stability

P. Boolchand and B. Goodman

The nature of glass transitions in chalcogenides and modified oxides depends on the network mean coordination number $\langle r \rangle$. These display systematic trends when spanning across the three topological phases: flexible, intermediate, and stressed-rigid. Trends in the glass-transition temperature $T_g(\langle r \rangle)$ show a monotonic increase with $\langle r \rangle$, but the nonreversing enthalpy of relaxation at T_g, $\Delta H_{nr}(\langle r \rangle)$, shows a deep- and square-well-like minimum with the walls representing the rigidity and stress transitions with increasing $\langle r \rangle$, respectively. In the well, the $\Delta H_{nr}(\langle r \rangle)$ term remains minuscule (~0) corresponding to the isostatically rigid intermediate phase (IP). The melt fragility index (m) shows rather low values, $m(\langle r \rangle) < 20$ for IP compositions, but increases outside the IP. Glass compositions in the IP show absence of network stress, form compacted networks, possess thermally reversing glass transitions, and display high glass-forming tendency—functionalities that have attracted widespread interest in understanding the physics of glasses and applications of the new IP formed.

Origin of glass-forming tendency

Ever since the inception of academic glass research, practitioners have often wondered—what is so special about the select few melts that can bypass crystallization and be supercooled to form bulk glasses at the glass-transition temperature (T_g)? With the important strides made in glass science in the past 35 years, both in theory and experiments, we now have a wealth of new information on the crucial role of network topology in decoding the origin of the glass-forming tendency.

The Phillips–Thorpe Rigidity Theory[1–3] has been pivotal in elucidating the physics of network glasses. The key parameter in the theory is the number of constraints per atom, n_c, due to chemical bonds, in particular, bond-stretching and bond-bending interactions. When $n_c = 3$, glassy networks are optimally constrained, fulfilling the Maxwell criteria for rigidity (i.e., $n_c = 3$ for three-dimensional networks). Such optimally constrained networks within the Phillips–Thorpe approach possess a mean coordination number of 2.40. At $n_c < 3$, networks possess low-frequency floppy modes and are flexible, those with $n_c > 3$, possess stress-creating redundant bonds and are stressed-rigid, while those with $n_c = 3$ form networks that belong to an intermediate phase (IP). The comparative functionalities of the underlined three topological phases have evoked much interest in glass science.

The first tests of these topology-driven ideas were applied to the chalcogenide glasses. These glasses represent alloys of Group VI (S, Se) elements with Group IV (Si, Ge) or Group V (P, As) elements. An attractive feature of these elements is that their chemical bonding conforms to the 8-N bonding rule, where N represents the number of valence electrons. Thus, the coordination number r acquired by Ge, As, and Se usually is 4, 3, and 2, respectively. One can thus enumerate the mechanical constraints per atom, n_c, from a knowledge of the chemical stoichiometry alone of an alloyed glass composition such as $Ge_xAs_ySe_{100-x-y}$.

Thermally reversing windows and birth of the IP

The most unusual nature of isostatically rigid networks came to the forefront when Raman scattering measurements and modulated differential scanning calorimetry (MDSC) experiments were performed in precise compositional studies of the chalcogenides.[4–6] Isostatically rigid networks are those in which optimally constrained local structures percolate across the glass sample. These experiments showed that IP networks do not form merely at one characteristic stoichiometry of $r_c = 2.40$, but rather, over a small but finite range of connectivity, the IP window $r_c^1 < \langle r \rangle < r_c^2$, near 2.40, with sharply defined edges r_c^1 and r_c^2 representing the rigidity and stress transitions, respectively. To obtain such sharp edges, it is crucial that the alloyed melt/glass batch be highly homogeneous.[7] Within the IP window, glasses possess

P. Boolchand, Department of ECS, College of Engineering and Applied Science, University of Cincinnati, USA; boolchp@ucmail.uc.edu
B. Goodman, Department of Physics, University of Cincinnati, USA; goodman.bernard@gmail.com
doi:10.1557/mrs.2016.300

unusual functionalities: (1) they form stress-free networks;[8] (2) they possess a near vanishing enthalpy of relaxation[9,10] at T_g, which ages minimally; (3) they form space-filling or compacted networks;[11] and (4) they display glass transitions that are thermally reversing in character.[4] The dynamic reversibility is the signature for self-organization of these glasses.

MDSC and nature of T_g

Differential scanning calorimetry (DSC) has been widely used[12] to establish T_g of glasses since the early 1960s. In a DSC experiment, a glass is heated typically at a linear scan rate of 20°C/min, and one observes a T_g endotherm, which broadly consists of (1) a rounded step on which is superposed (2) a Gaussian-like overshoot. The midpoint or inflection point of the step-like feature is usually taken as a measure of T_g, while the integrated area under the Gaussian profile provides a measure of enthalpy relaxation (ΔH_{nr}). One of the challenges in DSC is to reliably separate (1) the step feature from (2) the overshoot feature.

An alternating current (AC) variant known as MDSC (modulated DSC) was introduced[13] in the mid-1990s, wherein a sinusoidal temperature modulation on the linear scan rate leads to an endothermic heat flow similar to the one seen in DSC, but with several crucial refinements. The AC nature of MDSC permits the full power of phase-sensitive lock-in detection to be used, which permits the use of rather slow scan rates (0.5–5°C/min) without loss of signal, thus completely suppressing not only T_g upshifts, but also broadening of the T_g endotherm due to the high scan rates used in DSC.

More importantly, MDSC shows that the step-like feature (1), which tracks the T-modulation, appears in the reversing heat flow, while the overshoot feature (2), which does not track the T-modulation, appears quite separately as a nonreversing heat flow. That separation is of fundamental importance in glass science since the former (1) captures ergodic features (thermodynamics), while the latter (2) captures the nonergodic (nonequilibrium) ones characteristic of T_g. Experiments reveal that ΔH_{nr} vanishes in the IP, but increases as networks become nonisostatic ($|n_c - 3| > 0$); ΔH_{nr} is closely tied to aging and is altered by glass impurity content and glass heterogeneity.

The fundamental importance of ΔH_{nr} is as follows. When non-IP glass compositions age, their configurational entropy decreases, and leads ΔH_{nr} to increase. Furthermore, since ΔH_{nr} of non-IP compositions always exceed those in the IP ones, heterogeneous glasses will usually display a greater ΔH_{nr} than homogeneous ones, and will also show aging of ΔH_{nr}, even for IP compositions. Presence of bonded water as an impurity in glasses leads to dangling ends, changing the degrees of freedom and increasing ΔH_{nr}. The reversing heat flow yields the heat capacity difference, ΔC_p, between the supercooled melt and the glass, and is largely $\langle r \rangle$-independent.

Figure 1 shows a typical MDSC scan of a $Ge_{10}Se_{90}$ glass taken at a 3°C/min scan rate, 1°C modulation amplitude, and 100 s modulation period. For this flexible-phase glass composition, the scan shows enthalpy of relaxation, ΔH_{nr} (= 0.61(2) cal/g), and ΔC_p (= 0.031(6) cal/g/°C). A modulation-frequency independent ΔH_{nr} term is established by recording the endotherm in the heating cycle and subtracting the exotherm in the cooling cycle.[13]

One of the first MDSC studies on a chalcogenide was on the Si_xSe_{100-x} binary, before the crucial role of homogeneity was appreciated. It was found that $T_g(x)$ increased with Si content (**Figure 2**a), reflecting the progressive cross-linking of the polymeric Se_n chains by Si. There was, nonetheless, a strikingly abrupt reduction of $\Delta H_{nr}(x)$ by almost a factor of 10 near $x_c(1) = 20\%$, the rigidity transition (Figure 2b), and an equally spectacular recovery near $x_c(2) = 27\%$, the stress transition; $\Delta H_{nr}(x)$ was minuscule in between these two points. Thus ΔH_{nr} is a measure of the departure of a glass

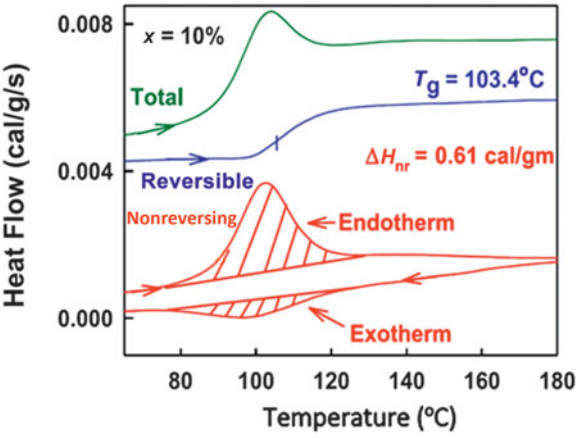

Figure 1. Modulated differential scanning calorimetry (MDSC) scan of $Ge_{10}Se_{90}$ glass showing the total, reversing, and nonreversing signals in the heating cycle.[7]

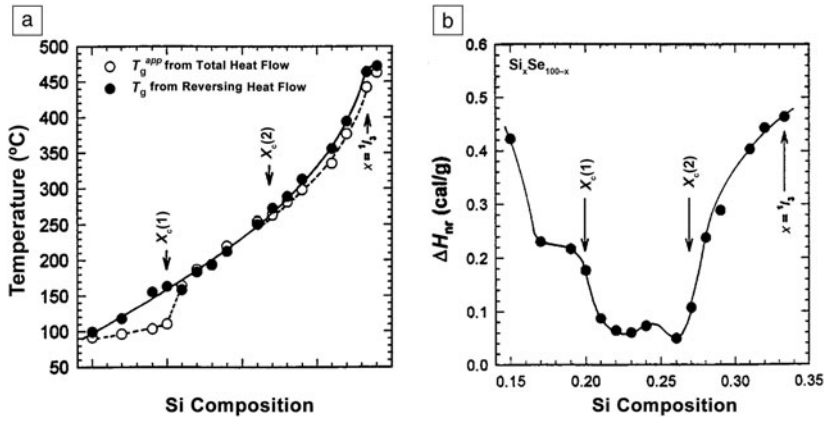

Figure 2. Trends in $T_g(x)$ and nonreversing enthalpy of relaxation in Si_xSe_{100-x} glasses, showing variation of $T_g(x)$ and $\Delta H_{nr}(x)$. The square-well like variation of $\Delta H_{nr}(x)$ shows walls at $x_c(1)$ and $x_c(2)$ representing the rigidity and stress transition.[4]

network from isostaticity. Such calorimetric windows have now been observed in more than 50 glass systems[14] and correlate with their optical, electrical, and mechanical properties. Characteristic power laws in Raman mode frequencies $\nu(x)$, and in low-frequency AC conductivity in solid electrolyte glasses also display compositional thresholds that coincide with the two elastic phase boundaries.

Slow homogenization of nonstoichiometric chalcogenide melts

Recently, FT-Raman profiling of chalcogenide melts during synthesis has elucidated the challenges in homogenizing nonstoichiometric glasses, even those of small sizes. A two-gram melt size homogeneously alloys over tens of days rather than hours. **Figure 3** shows FT-Raman profiling results for a $Ge_{19}Se_{81}$ batch composition encased in a 5-mm ID quartz tubing. Spectra recorded at nine equally spaced locations along the 1-in.-long melt column showed that the local vibrational density of states (measure of local[7] glass stoichiometry) of quenched melts varies significantly along the tube length even after reacting at 950°C for t_r = 96 h (Figure 3a). The Ge content x was deduced from the scattering strength ratio of the Se_n chain mode (250 cm^{-1}) to the corner-sharing mode (200 cm^{-1}), and displays a spread of about 6% in Ge content. At t_r = 168 h (Figure 3b), Raman profiling showed that melts were completely homogenized. In such homogeneous glasses, the reversibility window becomes square-well like,[15] with abrupt walls, and with the width of the rigidity and stress transitions becoming less than 0.5% in Ge content.[7,10]

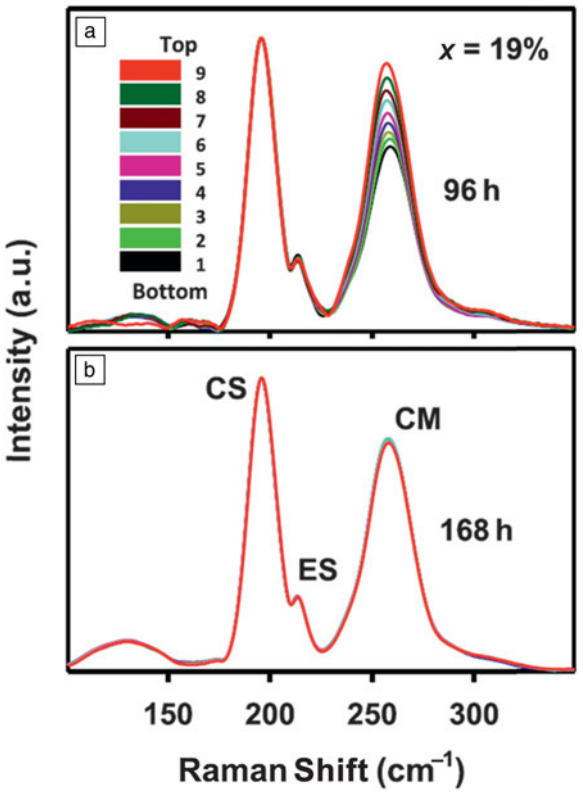

Figure 3. FT-Raman profile of a $Ge_{19}Se_{81}$ quenched melt taken (a) after 96 h (where x = Ge content) and (b) 168 h of reaction of Ge with Se.[7,15] Note: CS, corner-sharing mode of $GeSe_4$ tetrahedra; ES, edge-sharing mode of $GeSe_4$ tetrahedra; CM, chain mode of Se_n chains.

The long homogenization times reflect the fact that the viscosity of melts at the reaction temperature, particularly in the IP composition range, are at least one to two orders of magnitude greater than those of melt compositions outside the IP. Thus, the overall melt homogenization is being controlled by the higher viscosity phase in the IP. The recognition[16] emerged from the fragility index $m(x)$ of homogeneous melts. The fragility index is defined next.

Fragility windows and super-strong behavior of IP melt compositions

In MDSC, one may also choose to analyze the glass-transition endotherm in terms of the in-phase $Re(C_p)$ and out-of-phase $Im(C_p)$ components of the complex specific heat[17] instead of the reversing and nonreversing heat flows. The $Re(C_p)$ signal shows a step-like variation and tracks the modulations (akin to reversing heat flow), while the $Im(C_p)$ signal displays a Gaussian profile just as the nonreversing heat flow. There is a scaling factor (scan rate) that comes in since $Im(C_p)$ has units of a specific heat (cal/g/°C) while $\Delta H_{nr}(x)$ has units of heat flow (cal/g/s). By examining $Im(C_p)$ as a function of modulation frequency ω, one deduces the fragility index m of melts as follows. The peak in the $Im(C_p)$ signal corresponds to the condition $\omega\tau = 1$, where τ is the enthalpy relaxation time. At the peak in $Im(C_p)$ the melt has completely tracked the impressed modulation frequency (ω). Thus as ω increases, the peak in $Im(C_p)$ shifts to higher T. By plotting $\log_{10}\tau$ against $1/T$, one deduces an effective activation energy E_A of relaxation. The fragility index m at $T = T_g$ then follows from the following relation:

$$m = E_A/[T_g \ln 10]. \quad (1)$$

In Angell's well-known[18] display of $\log_{10}\eta$ versus $1/T$ for a variety of glass systems, those with $m < 20$ are associated with an Arrhenius-like behavior, $\eta(T) = A \exp(E_A/kT)$, and the effective activation energy $E_A(x,T)$ is independent of T. Here, A represents the value of η when $T = \infty$. In **Figure 4**, where the IP window is delineated in blue, we see that the melts there are super strong. Finally, since the fragility index (m) of non-IP melt always exceeds those in the IP, one expects heterogeneous melts to always display a greater m than homogeneous ones.

Extension of rigidity theory to oxide glasses

Rigidity theory started as a $T = 0$K description of the glassy state of matter. As the field evolved, it became clear that for SiO_2 glass, if, at the temperature T_g of nearly 1200°C, the

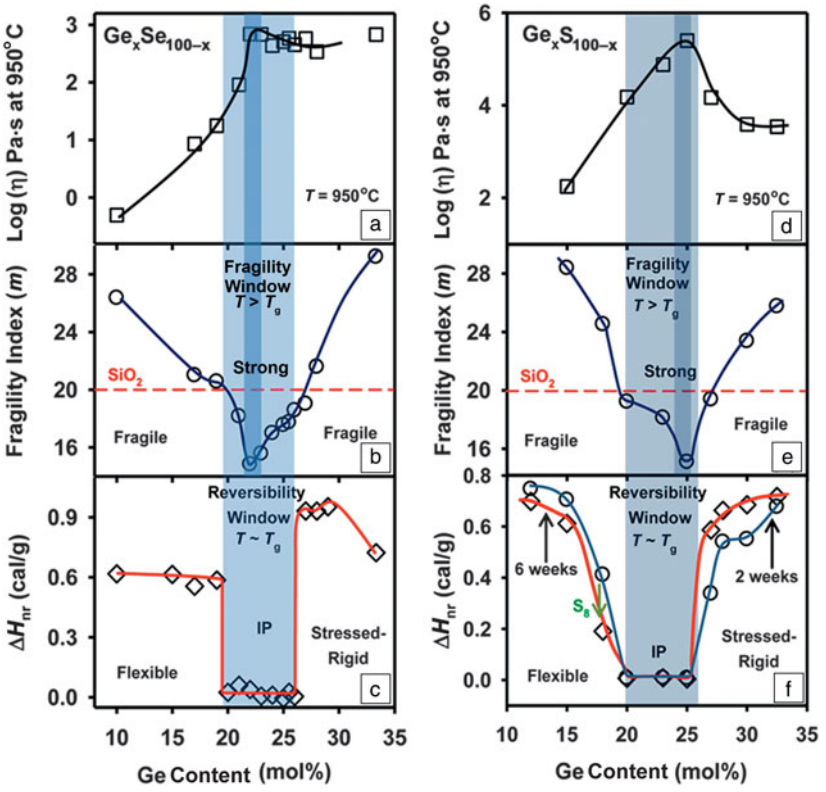

Figure 4. Variations in (a) estimated viscosity η(*x*) at 950°C, (b) measured fragility index, and (c) enthalpy of relaxation of homogeneous Ge_xSe_{100-x} glasses in left panel. (d–f) Corresponding data on Ge_xS_{100-x} glasses appear in the right panel.[10,16] Note: IP, intermediate phase.

weaker of the two bond-bending force constraints centered on oxygen were broken in the melt, the glass formed during the quench would be near isostatic (n_c = 3, or $\langle r \rangle$ = 2.40), thus accounting for its excellent glass-forming tendency.[19] The O-bond-bending force constraint is intact (broken) when the Si-O-Si bond angle has a fixed (variable) value. However, upon alloying 10 mol% of soda, T_g of sodium silicates rapidly decreases to almost 650°C, and one would expect the O-centered bond-bending constraints to be restored in the melt, driving the modified glass to now become stressed-rigid. Confirmation of that view was given by the observation of an IP in the 18%–23% range of soda that correlated nicely with Brillouin scattering deduced elastic constants.[20]

With the introduction of *T*-dependent constraints[21] along with molecular dynamics (MD) simulations[22] to confirm them, rigidity theory has evolved into a formidable quantitative tool for predicting[23] physical properties of commercial oxide glasses. It has also addressed a long-standing problem in the field of how to enumerate bonding constraints of monovalent (e.g., Li, Na, and K) and divalent (e.g., Ca, Sr, and Ba) modifiers in oxide glasses. The MD simulations[24] showed that in sodium silicates, although the Na^+ ion has a coordination number in the 5–6 range, the bond-stretching and bond-bending constraints with only one of the 5 or 6 oxygen near-neighbors are intact, while those with the rest of the oxygen near neighbors display a large variance in distance, suggesting that the underlying constraints are broken. Thus, one came to recognize that in estimating constraints in the modified oxides, the appropriate mechanically effective number of constraints is 1, consistent with its valence.

IP, ideal melts, and glasses

IPs have now been observed in several families of chalcogenide glasses[14] in polaronic conducting oxide glasses,[25] in solid electrolyte glasses,[26] in alkali-germanates, and in alkali[27] and alkaline-earth[28] borates. In the IPs, enthalpy of relaxation ΔH_{nr} almost vanishes, the boundaries become abrupt, and molar volumes show a global minimum. Furthermore, ΔH_{nr} ages minimally for IP compositions, in sharp contrast to compositions outside the IP. The stress-free nature of IPs is seen from pressure Raman experiments,[8] which show vibrational modes that blue-shift linearly for IP glass compositions, just as in crystalline solids, when an external pressure is applied. The observation underscores the absence of internal stress in IP glasses and in crystals. In ionic conductors, an exponential increase in conductivity appears only in the flexible phase where networks can easily deform because of floppy modes; in the IP, a new conductive regime sets in, which displays an anomalous behavior for typical jump distance as inferred by DC permittivity measurements. In Raman scattering, select vibrational modes blue-shift with composition, displaying a power-law in the IP and in the stressed-rigid phase.

Recently, a special effort using Raman profiling was made to synthesize homogeneous melts/glasses of the Ge-Se and Ge-S binary, and trends in $m(x)$, and $\Delta H_{nr}(x)$ were established using MDSC. In Figure 4, the upper two panels show the expected viscosity η(*x*) and the measured fragility index *m*(x) of the melt, while the lowest panel shows the nonreversing heat $\Delta H_{nr}(x)$ of the solid to melt transition. The IP window of the glass is delineated in blue. Figure 4 shows a remarkable correlation of super-strong ($m < 20$) melts with the IP. The viscosity η(*x*) is also the largest there, and the molar volume (not shown) the lowest for such glasses. The small $\Delta H_{nr}(x)$ seen in the lowest panels, for *x* in the IP, points to a remarkable correlation in that composition range between the structures of the solid and liquid. The thermodynamic relation $dH = TdS$, when integrated across the relatively small melting glass-transition temperature range in the MDSC, gives $\Delta H_{nr} = T_g(S_{melt} - S_{glass})$, so that the structural (configurational)

entropy (S_c) near T_g of IP glasses (S_{glass}) is almost the same as in their melts (S_{melt}). The larger values of $\Delta H_{nr}(x)$ outside the IP are taken to mean that their structures substantially change during melting. This gives us some insight, namely, that their isostatic subunits can rearrange themselves rather easily under thermal motion or shear stress while remaining connected, and so should persist into the melt phase above the IP, at least for temperatures low enough for the constraints to remain intact. This implies that the available configuration space for globally isostatic structures is relatively flat and easily sampled by diffusive motion. The glass should then be stress free and, most significantly, already aged. The statistical ensemble of such spaces leads to a relatively high entropy.

The plots of $\eta(x)$ on the top row of Figure 4 suggest why the homogenization kinetics of the initial melts are slow. This follows from the somewhat counterintuitive inverse behavior of $\eta(x)$ and the diffusion coefficient $D(x)$ as illustrated by the Stokes-Einstein relation, $\eta = k_B T/aD$ for a colloidal fluid mixture in which the variable a is the mean separation of colloidal particles. Recently,[29] MD simulations of Ge-Se melts have confirmed this relation in impressive detail. For x outside the IP window, there are spatially random interruptions of the isostatic structures that form localized barriers trapping the initially nonequilibrium available structures produced by the quenching to form an ensemble of relatively high entropy. Over time, thermal hopping will permit the ensemble to move toward equilibrium states of lower entropy and the window to become square-well like.

Returning to the question at the beginning of this article—What is so special about melts that so easily bypass crystallization even under slow air cooling? These inorganic alloy melts lie in or close to IP composition windows where networks are isostatically rigid. Their other physical features, such as showing much reduced aging, distinguish them as being in some sense "ideal" among glasses. The traditional notion[18] of ideality for glass seems to be related to the concept of the Kauzmann temperature at which the melt should supposedly reach the low configurational entropy of the crystalline phase. Our association of ideality with a high entropy phase confounds this notion, but still leaves us with the challenge of better understanding the IP.

Summary

Glasses of chalcogenides and modified oxides show common trends in calorimetric properties, Raman scattering, infrared reflectance, AC conductivity, and molar volumes as their connectivity or mean coordination number $\langle r \rangle$ increases in the $2 < \langle r \rangle < 3$ range. They all have three topological phases—flexible, intermediate, and stressed-rigid. Although T_g increases monotonically with $\langle r \rangle$, the enthalpy of relaxation at T_g shows a square-well like minimum with the walls representing the rigidity and stress transitions, respectively. For carefully homogenized melts, the glasses display a set of unusual properties, which earn their designation as being ideal. These include absence of network stress and compact networks with low-molar volumes. Additionally, they have a thermally reversing glass-to-melt transition, with corresponding melts displaying a high glass-forming tendency and with fragility index $m < 20$ (i.e., being super strong). Optical elastic power laws deduced from Raman scattering, and ionic-conductivity deduced from AC conductivity, reveal thresholds at the rigidity and stress transitions. These new functionalities are a consequence of the isostatically rigid nature of networks with $n_c = 3$.

Acknowledgments

This research was supported by the National Science Foundation (Grant DMR 08-53957). We thank K. Gunasekera, S. Bhosle, S. Chakraborty, C. Holbrook, R. Bhageria, K. Vignarooban, S. Dash, and S. Ravindren at the University of Cincinnati who have contributed to the experimental effort. We appreciate discussions with M. Micoulaut and C. McDonald during the course of this work.

References

1. J.C. Phillips, *J. Non Cryst. Solids* **34**, 153 (1979).
2. J.C. Maxwell, *Philos. Mag.* **27**, 294 (1864).
3. M.F. Thorpe, *J. Non Cryst. Solids* **57**, 355 (1983).
4. D. Selvanathan, W.J. Bresser, P. Boolchand, *Phys. Rev. B Condens. Matter* **61**, 15061 (2000).
5. X.W. Feng, W.J. Bresser, P. Boolchand, *Phys. Rev. Lett.* **78**, 4422 (1997).
6. P. Boolchand, D.G. Georgiev, B. Goodman, *J. Optoelectron. Adv. Mater.* **3**, 703 (2001).
7. S. Bhosle, K. Gunasekera, P. Boolchand, M. Micoulaut, *Int. J. Appl. Glass Sci.* **3**, 205 (2012).
8. F. Wang, S. Mamedov, P. Boolchand, B. Goodman, M. Chandrasekhar, *Phys. Rev. B Condens. Matter* **71**, 174201 (2005).
9. P. Boolchand, M. Jin, D.I. Novita, S. Chakravarty, *J. Raman Spectrosc.* **38**, 660 (2007).
10. S. Chakraborty, P. Boolchand, *J. Phys. Chem. B* **118**, 2249 (2014).
11. R. Bhageria, K. Gunasekera, P. Boolchand, M. Micoulaut, *Phys. Status Solidi B* **251**, 1322 (2014).
12. C.A. Angell, K.L. Ngai, G.B. McKenna, P.F. McMillan, S.W. Martin, *J. Appl. Phys.* **88**, 3113 (2000).
13. L.C. Thomas, *Modulated DSC Technology (MSDC-2006)* (TA Instruments, New Castle, DE, 2006).
14. B. Mantisi, M. Bauchy, M. Micoulaut, *Phys. Rev. B Condens. Matter* **92**, 134201 (2015).
15. S. Bhosle, K. Gunasekera, P. Boolchand, M. Micoulaut, *Int. J. Appl. Glass Sci.* **3**, 189 (2012).
16. K. Gunasekera, S. Bhosle, P. Boolchand, M. Micoulaut, *J. Chem. Phys.* **139**, (2013).
17. L. Carpentier, O. Bustin, M. Descamps, *J. Phys. D Appl. Phys.* **35**, 402 (2002).
18. C.A. Angell, D.R. Macfarlane, M. Oguni, *Ann. N.Y. Acad. Sci.* **484**, 241 (1986).
19. M. Zhang, P. Boolchand, *Science* **266**, 1355 (1994).
20. Y. Vaills, T. Qu, M. Micoulaut, F. Chaimbault, P. Boolchand, *J. Phys. Condens. Matter* **17**, 4889 (2005).
21. J.C. Mauro, P.K. Gupta, R.J. Loucks, *J. Chem. Phys.* **130**, 234503 (2009).
22. M. Micoulaut, *Adv. Phys. X* **1**,147 (2016).
23. J.C. Mauro, *Am. Ceram. Soc. Bull.* **90**, 31 (2011).
24. M. Bauchy, M. Micoulaut, M. Celino, S. Le Roux, M. Boero, C. Massobrio, *Phys. Rev. B Condens. Matter* **84**, 054201 (2011).
25. S. Chakraborty, P. Boolchand, M. Malki, M. Micoulaut, *J. Chem. Phys.* **140**, 014503 (2014).
26. D.I. Novita, P. Boolchand, M. Malki, M. Micoulaut, *J. Phys. Condens. Matter* **21**, 205106 (2009).
27. K. Vignarooban, P. Boolchand, M. Micoulaut, M. Malki, W.J. Bresser, *Europhys. Lett.* **108**, 56001 (2014).
28. C. Holbrook, S. Chakraborty, S. Ravindren, P. Boolchand, J.T. Goldstein, C.E. Stutz, *J. Chem. Phys.* **140**, 144506 (2014).
29. C. Yildirim, J.Y. Raty, M. Micoulaut, *Nat. Commun.* **7**, 11086 (2016). □

Punit Boolchand joined the University of Cincinnati in 1969 and is currently Professor of Electrical and Computer Engineering and Physics. He received his PhD degree in physics in 1969 from Case Western Reserve University. He has held visiting positions at Stanford University, University of Paris, France, and KU Leuven, Belgium. The new intermediate phase was observed in network glasses in 1998 at the University of Cincinnati. He is a Fellow of the American Physical Society and recipient of the Stanford Ovshinsky Award. Boolchand can be reached by phone at 513-556-4790 or by email at boolchp@ucmail.uc.edu.

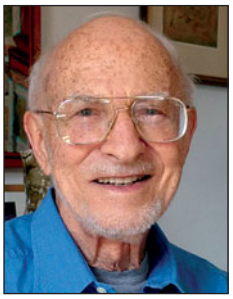

Bernard Goodman has been Professor Emeritus of Physics at the University of Cincinnati since 1993. He received his PhD degree in physics in 1955 from the University of Pennsylvania. After 13 years at the University of Missouri, he joined the University of Cincinnati in 1965 as a professor of physics. His expertise is in theory of condensed matter—many-body theory of electron correlations and lattice dynamics of disordered systems. He is a Fellow of the American Physical Society and has been a Guggenheim Fellow and Fulbright Fellow. He has been a Nordita Visiting Professor at two Swedish universities. Goodman can be reached by phone at 513-556-0537 or by email at goodman.bernard@gmail.com.